Thermal poling behavior and SHG stability in arsenic-germanium sulfide glasses

William T. Shoulders,[1,2] Jacklyn Novak,[3,5] Marc Dussauze,[4,*] J. David Musgraves,[3] and Kathleen Richardson[1,2,3]

[1]*Department of Materials Science and Engineering, University of Central Florida, 4000 Central Florida Blvd., Orlando, Florida 32816, USA*
[2]*College of Optics and Photonics, University of Central Florida, 4000 Central Florida Blvd, Orlando, Florida 32816, USA*
[3]*Department of Materials Science and Engineering, Clemson University, Clemson, South Carolina 29634, USA*
[4]*Université Bordeaux, ISM, CNRS UMR 5255, 33400 Talence, France*
[5]*Now with Lightpath Technologies, Orlando, Florida 32826, USA*
[*]*m.dussauze@ism.u-bordeaux1.fr*

Abstract: Second-order optical properties of thermally poled arsenic-germanium sulfide glasses have been investigated. Parallel studies of glass structure changes upon poling and/or visible cw-laser irradiation and complete SHG quantitative analysis have been performed. Key parameters and poling mechanisms influencing largely SHG stability and efficiency have been pointed out.

OCIS codes: (160.2750) Glass and other amorphous materials; (190.4400) Nonlinear optics, materials; (160.4330) Nonlinear optical materials.

References and links

1. B. J. Eggleton, B. Luther-Davies, and K. Richardson, "Chalcogenide photonics," Nat. Photonics **5**, 141–148 (2011).
2. Y. Sasaki and Y. Ohmori, "Phase-matched sum-frequency light generation in optical fibers," Appl. Phys. Lett. **39**(6), 466–468 (1981).
3. U. Österberg and W. Margulis, "Experimental studies on efficient frequency doubling in glass optical fibers," Opt. Lett. **12**(1), 57–59 (1987).
4. M. Guignard, V. Nazabal, F. Smektala, H. Zeghlache, A. Kudlinski, Y. Quiquempois, and G. Martinelli, "High second-order nonlinear susceptibility induced in chalcogenide glasses by thermal poling," Opt. Express **14**(4), 1524–1532 (2006).
5. M. Dussauze, X. L. Zheng, V. Rodriguez, E. Fargin, T. Cardinal, and F. Smektala, "Photosensitivity and second harmonic generation in chalcogenide arsenic sulfide poled glasses," Opt. Mater. Express **2**(1), 45–54 (2012).
6. H. Guo, X. Zheng, M. Lu, K. Zou, B. Peng, S. Gu, H. Liu, and X. Zhao, "Large second-order nonlinearity in thermally poled Ge-Sb-Cd-S chalcogenide glass," Opt. Mater. **31**(6), 865–869 (2009).
7. M. Dussauze, V. Rodriguez, A. Lipovskii, M. Petrov, C. Smith, K. Richardson, T. Cardinal, E. Fargin, and E. I. Kamitsos, "How does thermal poling affect the structure of soda-lime glass?" J. Phys. Chem. C **114**(29), 12754–12759 (2010).
8. P. Thamboon and D. M. Krol, "Second-order optical nonlinearities in thermally poled phosphate glasses," J. Appl. Phys. **93**(1), 32–37 (2003).
9. R. A. Myers, N. Mukherjee, and S. R. J. Brueck, "Large second-order nonlinearity in poled fused silica," Opt. Lett. **16**(22), 1732–1734 (1991).
10. M. Guignard, V. Nazabal, F. Smektala, J. L. Adam, O. Bohnke, C. Duverger, A. Moréac, H. Zeghlache, A. Kudlinski, G. Martinelli, and Y. Quiquempois, "Chalcogenide glasses based on germanium disulfide for second harmonic generation," Adv. Funct. Mater. **17**(16), 3284–3294 (2007).
11. M. Dussauze, T. Cremoux, F. Adamietz, V. Rodriguez, E. Fargin, G. Yang, and T. Cardinal, "Thermal poling of optical glasses: mechanisms and second-order optical properties," Int. J. Appl. Glass Sci. **3**(4), 309–320 (2012).
12. R. Jing, Y. Guang, Z. Huidan, C. Guorong, K. Tanaka, K. Fujita, S. Murai, and Y. Tsujiie, "Second-harmonic generation in thermally poled chalcohalide glass," Opt. Lett. **31**(23), 3492–3494 (2006).
13. N. Carlie, "A solution-based approach to the fabrication of novel chalcogenide glass materials and structures," in *Materials Science and Engineering* (Clemson University, Clemson, SC, 2010), p. 163.
14. C. Lopez, "Evaluation of the photo-induced structural mechanisms in chalcogenide glass," in *College of Optics and Photonics* (University of Central Florida, Orlando, FL, 2004).

#185244 - $15.00 USD Received 11 Feb 2013; revised 8 Apr 2013; accepted 9 Apr 2013; published 1 May 2013

15. V. Rodriguez, "Quantitative determination of linear and second-harmonic generation optical effective responses of achiral or chiral materials in planar structures: theory and materials," J. Chem. Phys. **128**(6), 064707–064710 (2008).
16. C. Maurel, L. Petit, M. Dussauze, E. I. Kamitsos, M. Couzi, T. Cardinal, A. C. Miller, H. Jain, and K. Richardson, "Processing and characterization of new oxysulfide glasses in the Ge–Ga–As–S–O system," J. Solid State Chem. **181**(10), 2869–2876 (2008).
17. A. T. Ward, "Raman spectroscopy of sulfur, sulfur-selenium, and sulfur-arsenic mixtures," J. Phys. Chem. **72**(12), 4133–4139 (1968).
18. G. Lucovsky, "Optic modes in amorphous As_2S_3 and As_2Se_3," Phys. Rev. B **6**(4), 1480–1489 (1972).
19. G. Lucovsky and R. M. Martin, "A molecular model for the vibrational modes in chalcogenide glasses," J. Non-Cryst. Solids **8–10**, 185–190 (1972).
20. M. Muniz-Miranda, G. Sbrana, P. Bonazzi, S. Menchetti, and G. Pratesi, "Spectroscopic investigation and normal mode analysis of As_4S_4 polymorphs," Spectrochim. Acta A Mol. Biomol. Spectrosc. **52**(11), 1391–1401 (1996).
21. K. Tanaka, "Photo-induced phenomena in chalcogenide glass: comparison with those in oxide glass and polymer," J. Non-Cryst. Solids **352**(23-25), 2580–2584 (2006).
22. L. Calvez, Z. Yang, and P. Lucas, "Composition dependence and reversibility of photoinduced refractive index changes in chalcogenide glass," J. Phys. D Appl. Phys. **43**(44), 445401 (2010).
23. H. Fritzsche, "The origin of reversible and irreversible photostructural changes in chalcogenide glasses," Philos. Mag. B **68**, 561–572 (1993).
24. D. L. Douglass, C. C. Shing, and G. Wang, "The light-induced alteration of realgar to pararealgar," Am. Mineral. **77**, 1266–1274 (1992).
25. K. Trentelman, L. Stodulski, and M. Pavlosky, "Characterization of pararealgar and other light-induced transformation products from realgar by Raman micro spectroscopy," Anal. Chem. **68**(10), 1755–1761 (1996).
26. H. Kobayashi, H. Kanbara, M. Koga, and K. Kubodera, "Third-order nonlinear optical properties of As_2S_3 chalcogenide glass," J. Appl. Phys. **74**(6), 3683–3687 (1993).
27. R. H. Stolen and H. W. K. Tom, "Self-organized phase-matched harmonic generation in optical fibers," Opt. Lett. **12**(8), 585–587 (1987).
28. T. G. Alley, S. R. J. Brueck, and M. Wiedenbeck, "Secondary ion mass spectrometry study of space-charge formation in thermally poled fused silica," J. Appl. Phys. **86**(12), 6634–6640 (1999).
29. T. G. Alley, S. R. J. Brueck, and R. A. Myers, "Space charge dynamics in thermally poled fused silica," J. Non-Cryst. Solids **242**(2-3), 165–176 (1998).
30. D. Faccio, V. Pruneri, and P. G. Kazansky, "Dynamics of the second-order nonlinearity in thermally poled silica glass," Appl. Phys. Lett. **79**(17), 2687–2689 (2001).
31. M. Dussauze, E. Fargin, M. Lahaye, V. Rodriguez, and F. Adamietz, "Large second-harmonic generation of thermally poled sodium borophosphate glasses," Opt. Express **13**(11), 4064–4069 (2005).
32. M. Dussauze, E. I. Kamitsos, E. Fargin, and V. Rodriguez, "Structural rearrangements and second-order optical response in the space charge layer of thermally poled sodium–niobium borophosphate glasses," J. Phys. Chem. C **111**(39), 14560–14566 (2007).
33. K. Shimakawa, S. Inami, and S. R. Elliott, "Reversible photoinduced change of photoconductivity in amorphous chalcogenide films," Phys. Rev. B Condens. Matter **42**(18), 11857–11861 (1990).

1. Introduction

Manufacturing compact optical components in an age in which the scale of devices continues to shrink will rely on novel functional materials. Of particular interest are materials exhibiting high second- and third-order optical nonlinearities to be leveraged in applications such as frequency conversion, beam splitting, and optical switching. The usefulness of infrared transmissive materials such as chalcogenide glasses for the aforementioned applications in, for instance, sensing devices has attracted attention lately [1]. Although the wide transmission window of chalcogenide glasses is well suited for infrared wave guiding, producing any second-harmonic frequency is largely forbidden due to the effective centro-symmetry of glassy structures. Even in fibers, where sum frequencies and second-harmonic generation (SHG) might be expected to result from multiple mode propagation, these effects are still minimal [2]. Various processing routes have been demonstrated to break the centro-symmetry of the glass network [3]. In this paper we focus on the unique effects of the thermal poling processes, which open up the possibility of new function in scalable forms (bulk, thin film, and/or fiber) of glass.

Over the past 25 years, thermal poling studies have been conducted on silicate, phosphate, and most recently chalcogenide glasses [4–8]. The general procedure for thermal poling, first described by Myers, involves the application of an electric field across a specimen at an

#185244 - $15.00 USD Received 11 Feb 2013; revised 8 Apr 2013; accepted 9 Apr 2013; published 1 May 2013

elevated temperature followed by cooling to room temperature at constant field [9]. It is well established that this polarization process embeds a static electric field within the glass matrix, triggered by the formation of a depletion layer of mobile cations at the anode surface of the poled sample. Nevertheless, from past studies of thermal poling, there is a definite consensus that depending on the initial composition of the poled glass, cationic, anionic, as well as electronic charge motion can all play a major role in the poling mechanism [10,11]. Another major part of the story is the temporal stability of the SHG, which varies greatly for materials such as silica and other oxide glasses, and also in the focus of this study, chalcogenide glasses (ChGs). Specifically in poled chalcogenide glasses, the temporal stability varies widely in the literature [10,12].

The two issues of primary importance in order to bring poled glass technology into greater use in optical systems are: (1) the magnitude of the induced $\chi^{(2)}$ and (2) its subsequent temporal stability (or ability to be long-lived) following removal of the applied field and under post-poling ambient conditions. Many efforts to achieve high temporal stability focus heavily on the processing. Although the processing step is important, we find it necessary to draw on our experience with glass chemistry as well as the poling mechanisms to propose a route towards high temporal stability. In this study, the evolution of glass structure from its initial state, through a thermal poling process is shown to play a major role in determining the temporal stability of SHG in a post-poled glass. The focus of the effort was not to maximize the magnitude of the induced χ^2, but rather, to understand the mechanism of the process within a multi-component chalcogenide glass to determine possible means to maximize its post-poling temporal stability through selective modification of the poled glass network.

In this study, we investigate two glass compositions, $As_{36}Ge_6S_{58}$ and $As_{34}Ge_6Na_2S_{58,}$ and compare their poling behavior, namely the temporal stability of the induced SHG and the poling induced structural rearrangements. The parent glass, $As_{36}Ge_6S_{58}$, was chosen for its well-known photosensitivity and its known structural reorganization which occurs upon exposure to laser irradiation [13]. The composition with 2 mol% sodium was chosen for its expected higher ionic conductivity and thus the expected alkali ion (cation) migration's role in the poling mechanism. Parallel studies of glass structure changes upon poling and/or visible cw-laser irradiation, and complete SHG quantitative analysis have been performed. Key parameters and poling mechanisms influencing largely SHG stability and efficiency have been pointed out.

2. Experimental

2.1 Glass synthesis

Glasses were made by batching appropriate molar quantities of elemental arsenic, germanium, and sulfur, along with sodium (II) sulfide in a nitrogen containing glove box. Batch chemicals were transferred to fused silica ampoules [13]. The ampoules were evacuated under vacuum and sealed with a gas torch to prepare for melting. Ampoules were placed in a rocking furnace for 14 hours at 850°C. The glasses were quenched in air, and then annealed in air at 180°C for 12 hours. Details on the glass synthesis can be found elsewhere [14]. Glass rods were cut and optically polished into 2 mm thick windows for poling experiments.

2.2 Poling

Poling treatments were done in argon atmosphere. Silicon electrodes were placed on each side of the glass samples to ensure good electrical contact and a uniform electric field across a 2 mm^2 poled region. The chalcogenide glass slides were heated to a poling temperature of 150°C and polarized with a voltage of 1.5 kV applied for 30 min after the poling temperature was reached. The voltage remained constant until the sample cooled down to room temperature.

#185244 - $15.00 USD Received 11 Feb 2013; revised 8 Apr 2013; accepted 9 Apr 2013; published 1 May 2013

2.3 Structural characterization

The structure of the glasses before and after poling treatments was studied by micro-Raman spectroscopy using a HR800 Horiba/Jobin–Yvon spectrometer working in backscattering geometry using the 752 nm excitation line of a solid-state laser with a typical spectral resolution of 3 cm^{-1}. The spectrophotometer included a holographic Notch filter for Rayleigh rejection, a microscope equipped with a 100× objective, and a CCD air-cooled detector. A low power of 1 mW was used to ensure no photo-induced alteration of the sample ensued. The photosensitivity of the glasses was studied by irradiating the samples with the same 752 nm source operating at 10 mW.

2.4 Characterization of second harmonic

Polarized SHG Maker fringe patterns were recorded using an OPO intra-cavity laser operating at 1550 nm, at low irradiance; depending on the experiments, a maximum energy on the sample of 200 μJ was used. The pulse width and the repetition rate of laser pulses were about 10 ns and 30 Hz, respectively. The fundamental intensity was monitored using a fiber with a large numerical aperture placed close to a mirror to collect the scattered fundamental light quantified by an InGaAs photodiode connected at the output of the fiber. Second-harmonic generation (SHG)-transmitted signals were detected by a photomultiplier and averaged over 50 pulses. Two different measurements were carried out. First, SHG kinetic measurements were performed under a continuous laser irradiation with p-p polarization configurations, i.e., p-polarized incident pump beam and p-polarized transmitted second-harmonic beam to determine the SHG stability as a function of the laser irradiation at 1550 nm. Second, quantitative macro-SHG measurements were made in transmission under continuous scans of both the incident angle value (θ-scans) with a fixed laser polarization and the input beam polarization Πψ-scans) at a fixed angle of incidence θ. This procedure contains at least four separate experiments which have been fitted simultaneously using the same set of parameters and an optical model based on an optical transfer matrix procedure [15].

3. Results

The time-dependent SHG signal was measured immediately following the poling treatments. Figure 1 shows the results obtained for the two $As_{36}Ge_6S_{58}$ and $As_{34}Ge_6Na_2S_{58}$ poled glass samples. A very fast decay of the SHG signal for Na-free poled samples can be observed. Very similar behavior has been observed by some in As_2S_3 poled samples [5]. On the contrary, the samples containing 2 mol% of sodium exhibit a stable SHG signal upon a 200 μJ irradiation at 1550 nm. After twenty days, the SHG signal probed at the same position remain unaffected. Twelve months after poling, the $As_{34}Ge_6Na_2S_{58}$ SHG signal is still stable. The small intensity decrease observed was attributed to the sample inhomogeneity. Several additional parameters are needed to develop an accurate optical model. The complete characterization of the SHG response will be presented in the next section of the paper.

#185244 - $15.00 USD Received 11 Feb 2013; revised 8 Apr 2013; accepted 9 Apr 2013; published 1 May 2013

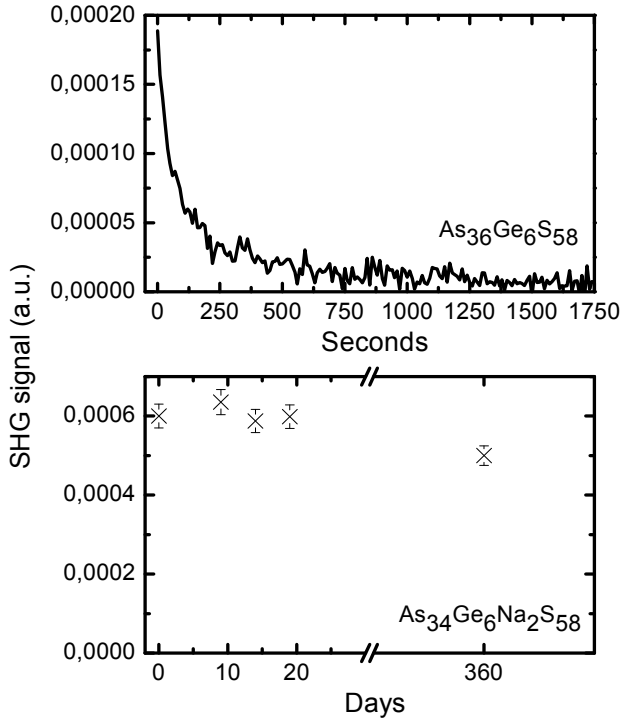

Fig. 1. SHG signal kinetics of $As_{36}Ge_6S_{58}$ (up) and $As_{34}Ge_6Na_2S_{58}$ (down) poled samples.

In analogy to a previous study which has pointed out close similarities between poling and photosensitivity mechanisms, the glass structure was studied under four different conditions: 1) following the annealing step of the glass synthesis, 2) following the exposure of samples to higher power sub-band gap cw light, 3) after poling treatment, and finally 4) following a second irradiation on the poled region of the sample [5].

The photo-structural changes induced in the$As_{34}Ge_6Na_2S_{58}$ chalcogenide glasses are reported in Fig. 2. All the Raman spectra exhibit a broad band centered at 340 cm^{-1} attributed to As-S vibrations in As-$S_{3/2}$ pyramidal sites which overlap an expected smaller contribution from Ge-S bonds vibrational mode of corner-sharing $GeS_{4/2}$units [16]. An additional shoulder at 360 cm^{-1} and vibrational modes at 233, 222, and 186 cm^{-1} can be observed. These additional contributions are typical of As-rich compositions and were attributed to As-As homo-polar bonds [17–20]. This initial data demonstrates that the as-melted $As_{34}Ge_6Na_2S_{58}$glass is slightly deficient in sulfur. After irradiation at 752 nm with 10 mW several spectral variations can be observed; notably, an intensity decrease at 360, 222, and 186 cm^{-1} and an intensity increase of the band peaking at 233 cm^{-1}. The photo-induced structural changes impact the modes linked to structural units with As-As homo-polar bonding such as As_4S_4. These spectral variations are in very good agreement with previous studies on photo-induced structural rearrangements in arsenic-based chalcogenide glasses [21–23]. Furthermore, the spectral variations observed upon laser irradiation have very close similarities with the data published in the mineralogist community on the polymorphic transition of As_4S_4 structural units from the realgar to para-realgar structure induced by simple visible light exposure [24,25].

#185244 - $15.00 USD Received 11 Feb 2013; revised 8 Apr 2013; accepted 9 Apr 2013; published 1 May 2013

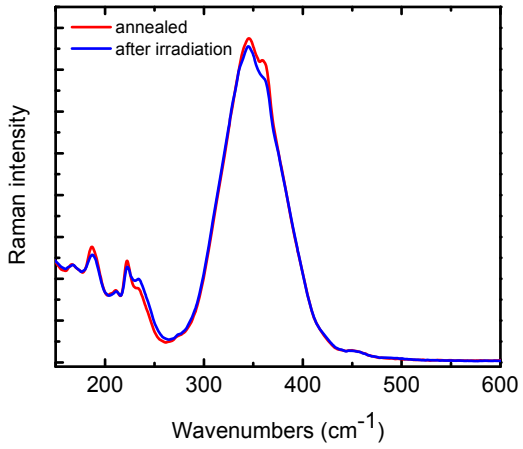

Fig. 2. Raman spectrum of an annealed $As_{34}Ge_6Na_2S_{58}$ sample overlaid with a Raman spectrum collected following sub-bandgap irradiation (752 nm, 10 mW).

We now focus on the effect of thermal poling on the $As_{34}Ge_6Na_2S_{58}$ polarized glassy network. The poled glass sample was divided in half and examined in cross section. As shown in Fig. 3(a), three distinct Raman spectra have been measured, starting at the anode surface and moving into the bulk glass. Similar to the spectral variations observed upon cw laser irradiation (refer to Fig. 2), the main changes are an intensity decrease at 360, 222, and 186 cm^{-1} and an intensity increase of the band peaking at 233 cm^{-1}. In Fig. 3(b), an image depicting the ratio of Raman intensities $I_{@233\ cm^{-1}}/ I_{@222\ cm^{-1}}$ measured on the cross section is shown (The good quality of our data permits to use a simple methodology which takes real Raman intensities without any fitting or baseline corrections). Two distinct structural layers can be observed: the first one starting at the anode surface [y = 0 in Fig. 3(b)] with a thickness of 5 µm exhibiting the largest spectral variations and a second layer with intermediate modification of the Raman activity forming a plateau up to 30 µm below the anode and slowly decreasing to reach the initial (or bulk) Raman spectra 40 µm below the surface.

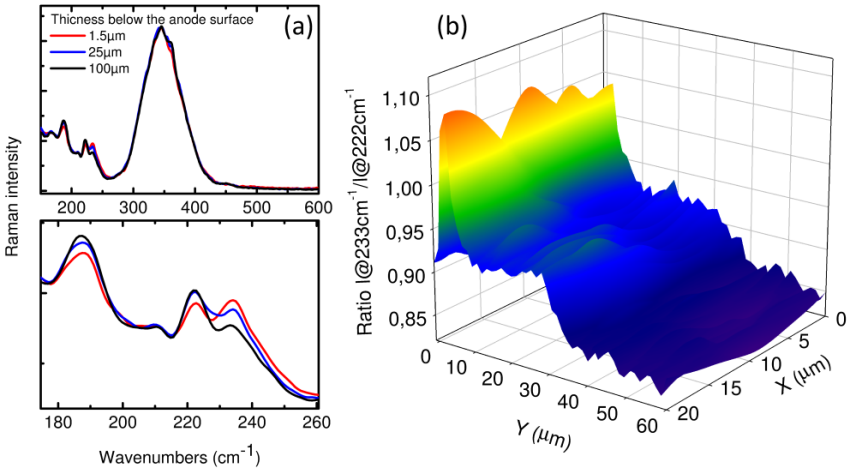

Fig. 3. (a) Raman spectra collected on the cross section of the $As_{34}Ge_6Na_2S_{58}$ poled sample. (b) Raman map of the anode cross section showing the evolution of the intensity ratio: $I_{@233\ cm^{-1}}/ I_{@222\ cm^{-1}}$.

#185244 - $15.00 USD Received 11 Feb 2013; revised 8 Apr 2013; accepted 9 Apr 2013; published 1 May 2013

Finally, to study photo-induced structural rearrangements of the $As_{34}Ge_6Na_2S_{58}$ poled glass, the irradiation procedure detailed above has been carried out at three different positions on the poled glass cross section, corresponding respectively to the two first poling-modified layers (i.e., Y = 1.5 µm and Y = 25 µm below the anode surface) and to the bulk glass as reference (Y = 100 µm). We first consider the different kinetics of the photo-induced structural rearrangements depicted in Fig. 4(a). For the bulk reference (Y = 100 µm) and the second layer (Y = 25 µm) a similar exponential decrease is observed. The only difference appears to be the starting point of the decay. During the measurement, the photochemical process stabilizes after 800 s for the two curves. Contrary to the first two layers, a minor decrease is observed in the third layer (Y = 1.5 µm) during the first minute followed by a stable trend. To better understand the spectral variation induced by irradiation in this anodic-poled layer, we compare, from Fig. 4(b), the Raman signature of the poled layer before and after the irradiation process with the reference spectrum of the bulk glass. As observed in the kinetic curve, a small change in the relative intensities of the Raman bands at 222 and 233 cm^{-1} can be noticed, but the main effect clearly appears on the broadness of these two bands which significantly increase upon irradiation.

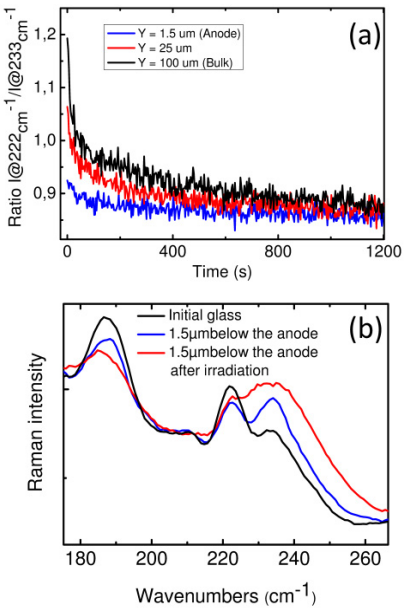

Fig. 4. (a) Raman intensity ratio ($I_{222\ cm\text{-}1}/I_{233\ cm\text{-}1}$) measured during the irradiation process at different positions on the $As_{34}Ge_6Na_2S_{58}$ poled sample cross section. (b) Raman spectra of the initial $As_{34}Ge_6Na_2S_{58}$ glass sample, after poling 1.5 µm under the anode surface and the same position after an irradiation at 752 nm with 10 mW.

4. Discussion

4.1 Origin and quantification of the SHG response

The local symmetry of a poled glass belongs to the $C_{\infty v}$ point group, which is a polar uniaxial group oriented along the applied DC field. Consequently, assuming Kleinman's condition which is realistic in common glasses, only two independent components, $\chi^{(2)}_{zzz}$ and $\chi^{(2)}_{zxx} = \chi^{(2)}_{xzz}$, are expected. In addition, by performing complete polarization scans as described in

#185244 - $15.00 USD Received 11 Feb 2013; revised 8 Apr 2013; accepted 9 Apr 2013; published 1 May 2013

the experimental section, we can characterize with precision the ratio $\chi^{(2)}_{zzz}/\chi^{(2)}_{zxx}$ and thus determine if the second-order optical response differs from an electric field-induced second-harmonic (EFISH) mechanism in an isotropic material which impose by symmetry requirement of the third-order nonlinear dielectric susceptibility tensor the ratio: $\chi^{(2)}_{zxx}/\chi^{(2)}_{zzz} = 1/3$.

Moreover, to perform a quantitative analysis of the $\chi^{(2)}$ tensor components, the optical model should at least integrate accurate values of the refractive indices at ω and 2 ω and the thickness of the NLO layer. Raman data have shown that the effect of the poling treatment on the glass network occurs in two well-defined layers below the anode surface [see Fig. 3(b)]. On the Maker fringes pattern recorded, strong over modulation on the top of a large envelope can be observed [θ-scan Fig. 5(a)]. Such signal is typical of optical interferences occurring between two SHG-active layers with a large difference in thicknesses, which could be attributed to (i) a thin anodic layer and (ii) a bulk SHG responses. Finally an optical model satisfying the zero potential condition with two SHG-active zones has been developed as described elsewhere [11]. All the experimental and calculated SHG patterns are depicted in Fig. 5. In this study, the only experimental data which can be sensitive to a change in the NLO layer thicknesses is the θ-scan, which induces continuous changes of the optical pathway forming SHG interference patterns. Two similar solutions have been obtained for different values of the anodic layer thickness (t = 3.9 μm and t = 37 μm). Such results can be directly attributed to the fact that the thickness of the NLO active layer at the anode is not sufficiently large as compared to the coherence length and does not give an accurate value of the effective $\chi^{(2)}$ induced by poling in this glass. Finally, without additional experimental evidence of the anodic SHG profile, we can only conclude on the order of magnitude of the response which is $\chi^{(2)} = 5.10^{-2}$ pm/V.

Now we shift focus to the SHG polarization scans [ψ-scans in Fig. 5(b)]. A very close agreement between fitted and experimental curves has been obtained for the $\chi^{(2)}_{zxx}/\chi^{(2)}_{zzz}$ ratio, which is exactly equal to 1/3. This proves that the origin of the second-order optical properties is clearly an electro-optical EFISH effect resulting from the interaction of the embedded electric field at the near-anode surface and the third-order optical susceptibility of the glass [9] ($\chi^{(2)} = 3\chi^{(3)}E_{stat}$). E_{stat} is the strength of the embedded electric field. Using a value of $\chi^{(3)}$ for As_2S_3 from the literature ($5.6\ 10^{-19}$ m^2/V^2) to approximate the $\chi^{(3)}$ of our samples and a $\chi^{(2)}$ on the order of 5.10^{-2}pm/V, the electric field predicted is 3.10^4 V/m [26,27]. Such a value is four orders of magnitude lower than the electric field strength implemented in poled silica of the Infrasil type [11]. This suggests that a fully effective implementation of the static electric field was not successfully achieved.

#185244 - $15.00 USD Received 11 Feb 2013; revised 8 Apr 2013; accepted 9 Apr 2013; published 1 May 2013

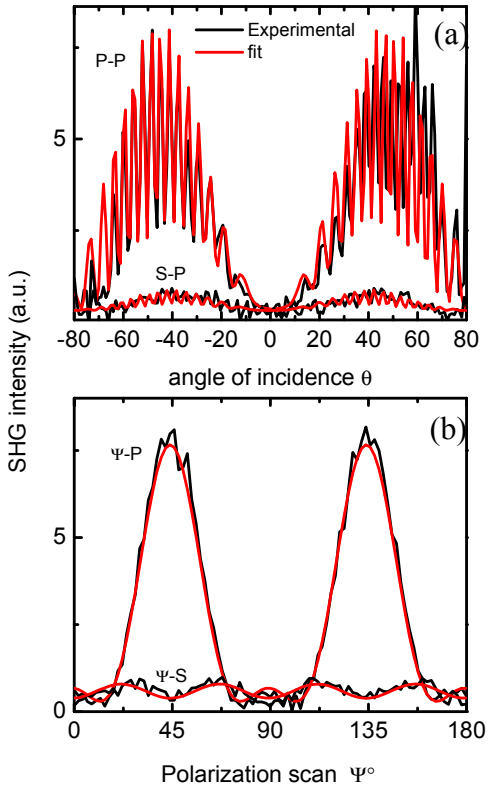

Fig. 5. Experimental (black) and calculated (red) profiles for transmitted P-P (S-P) Maker fringes pattern (a) and continuous polarization scan patterns ψ-P (ψ-S) obtained at an angle of 55° (b) of a $As_{34}Ge_6Na_2S_{58}$ poled glass.

Polarization mechanisms in glasses are dictated by charge rearrangement processes that are triggered by a depletion of mobile cations formed in a micrometer-sized layer below the anode surface [28–31]. In the sodium containing glass studied, if we assume the formation of a sodium depletion layer at the anode, the positive charge per volume displaced can be estimated to be around ~10^8 C/m^3. The electric field strength has been estimated at 3.10^4 V/m, which gives a final charge density within the space charge layer on the order of 1 to 10 C/m^3 with the uncertainty of the polarized layer thickness [32]. Thus, for poling treatments carried out in a neutral atmosphere, an additional displacement of negative charge carriers from the glass network takes place to compensate for the excess of negative charges created by sodium depletion. The well-known electronic conduction in chalcogenide glasses accommodates this mechanism. In the sodium containing chalcogenide glass, the poling treatment could be simply described as a continual generation of negative charges formed by the cations displacement towards the cathode and compensated by electronic conduction. By cooling the sample, both electronic and ionic conductivity decrease, which allows entrapping negative local charges to screen one part of the applied field within the glass matrix below the anode surface. Finally, to explain the relatively low strength of the embedded electric field as compared to oxide glasses, one should consider that both charge carriers' conductivities (i.e., cationic and electronic conduction) are similarly activated by the poling conditions.

#185244 - $15.00 USD Received 11 Feb 2013; revised 8 Apr 2013; accepted 9 Apr 2013; published 1 May 2013

4.2 SHG stability and structural rearrangements

Opposite to what has been reported for poled As_2S_3glasses [5] and observed for the $As_{36}Ge_6S_{58}$ composition (Fig. 1), the key result of this study concerns the time stability of the SHG signal in poled $As_{34}Ge_6Na_2S_{58}$ glasses. Moreover, it is important that the poled As_2S_3 study demonstrates that a thermal poling can induce a kinetic increase of the photo-induced structural rearrangements, which were related to charge defects created during the poling treatment. According to Shimakawa, upon the irradiation of chalcogenide glasses, unstable self-trapped excitons (or intimate charge defects) are created first [33]. These are then stabilized through reorganization of the glass matrix which separates them to form random pairs of charge defects. Using this simple but realistic description for thermally poled As_2S_3 and $As_{36}Ge_6S_{58}$ glasses, the space charge within the glass matrix is mainly implemented by the formation of unstable charge defects (similar to the self-trapped excitons formed during irradiation). These can serve to accelerate the photo-induced structural rearrangements but can also be easily erased, explaining the very low stability of the SHG signal induced by poling.

In $As_{34}Ge_6Na_2S_{58}$, the presented Raman data (see Fig. 4) clearly denotes high similarities between the structural changes induced by poling and irradiation. It tends to show that the large displacement of charges occurring during the polarization treatment of this sodium-rich glass composition (see discussion above) has driven the transition from the formation of unstable charge defects towards stabilized charges within a reorganized glass matrix to a saturation point. This is an important point as we try to understand the similarity of the poling and photo-induced structural changes mechanisms.

Finally, the SHG stability in poled arsenic sulfide-based glasses is directly linked to the nature of the local charges formed during the space charge implementation. Similar to the mechanisms of photosensitivity, these charges can be stabilized by forcing a self-reorganization of the glass matrix which occurs if the global charge density displaced upon the polarization treatment is sufficient for the sodium-rich glass in the present study.

5. Conclusion

This study of thermally poled sodium containing arsenic germanium sulfide glasses is the first to our knowledge to demonstrate the long-term temporal stability of SHG in a chalcogenide glass through the leveraging of structural changes brought about by the thermal poling process. These poling-induced structural changes bear resemblance to the photo-induced structural changes at 1550 nm. Glass compositions used in previous studies have not been ideal candidates for SHG due to the instability of the charge defects created by thermal poling. The glass of primary interest in this study, $As_{34}Ge_6Na_2S_{58}$, exhibited an effective second-order nonlinear susceptibility ($\chi^{(2)}$) on the order of 5.10^{-2} pm/V calculated according to the EFISH model. The SHG signal has been measured 12 months following the thermal poling treatment and no significant signal decay is detected. Additional work must be done to improve the magnitude of $\chi^{(2)}$ in chalcogenide glasses.

Acknowledgments

Funding to the Clemson (and now UCF) researchers has been provided in part by the National Science Foundation International REU program (ENG- 0649230). Additional support has been provided by the ATLANTIS - MILMI program with support from the US Department of Education of the United States Government under the contract #P116J080033 and the European Commission under the contract #2008-1750/001-001 CPT-USTRAN, Université Bordeaux 1. Funding to the University of Bordeaux and CNRS researchers has been provided in part by Région Aquitaine (LASINOF project: Advanced Materials in Aquitaine) and by AgenceNationale de la Recherche (project PolarChem ANR-2010 JCJC-0806 01). Partial support has been provided by the US Department of Energy (Contract # DE- NA000421),

NNSA/DNN R&D. This paper has been prepared as an account of work partially supported by an agency of the United States Government.

#185244 - $15.00 USD Received 11 Feb 2013; revised 8 Apr 2013; accepted 9 Apr 2013; published 1 May 2013